The Journal of Immunology

Correction of MFG-E8 Resolves Inflammation and Promotes Cutaneous Wound Healing in Diabetes

Amitava Das, Subhadip Ghatak, Mithun Sinha, Scott Chaffee, Noha S. Ahmed, Narasimham L. Parinandi, Eric S. Wohleb, John F. Sheridan, Chandan K. Sen and Sashwati Roy

J Immunol 2016; 196:5089-5100; Prepublished online 18 May 2016;
doi: 10.4049/jimmunol.1502270
http://www.jimmunol.org/content/196/12/5089

The Journal of Immunology is published twice each month by
The American Association of Immunologists, Inc.,
1451 Rockville Pike, Suite 650, Rockville, MD 20852

Print ISSN: 0022-1767 Online ISSN: 1550-6606.

Correction of MFG-E8 Resolves Inflammation and Promotes Cutaneous Wound Healing in Diabetes

Amitava Das,[*,†,‡] Subhadip Ghatak,[*,†,‡] Mithun Sinha,[*,†,‡] Scott Chaffee,[*,†,‡] Noha S. Ahmed,[*,†,‡] Narasimham L. Parinandi,[†,§] Eric S. Wohleb,[¶] John F. Sheridan,[¶] Chandan K. Sen,[*,†,‡] and Sashwati Roy[*,†,‡]

Milk fat globule epidermal growth factor-factor 8 (MFG-E8) is a peripheral glycoprotein that acts as a bridging molecule between the macrophage and apoptotic cells, thus executing a pivotal role in the scavenging of apoptotic cells from affected tissue. We have previously reported that apoptotic cell clearance activity or efferocytosis is compromised in diabetic wound macrophages. In this work, we test the hypothesis that MFG-E8 helps resolve inflammation, supports angiogenesis, and accelerates wound closure. MFG-E8$^{-/-}$ mice displayed impaired efferocytosis associated with exaggerated inflammatory response, poor angiogenesis, and wound closure. Wound macrophage-derived MFG-E8 was recognized as a critical driver of wound angiogenesis. Transplantation of MFG-E8$^{-/-}$ bone marrow to MFG-E8$^{+/+}$ mice resulted in impaired wound closure and compromised wound vascularization. In contrast, MFG-E8$^{-/-}$ mice that received wild-type bone marrow showed improved wound closure and improved wound vascularization. Hyperglycemia and exposure to advanced glycated end products inactivated MFG-E8, recognizing a key mechanism that complicates diabetic wound healing. Diabetic db/db mice suffered from impaired efferocytosis accompanied with persistent inflammation and slow wound closure. Topical recombinant MFG-E8 induced resolution of wound inflammation, improvements in angiogenesis, and acceleration of closure, upholding the potential of MFG-E8–directed therapeutics in diabetic wound care. ***The Journal of Immunology*****, 2016, 196: 5089–5100.**

Diabetic ulcer is a serious complication associated with type 2 diabetes mellitus (1, 2). A chronic inflammatory state is a characteristic feature of these ulcers (3, 4). Inflammation, an integral component of wound repair, defends against invading microbes and supports tissue repair through delivery of healing factors by blood-borne cells (5). Resolution of inflammation is a dynamically regulated process, the timeliness of which has major bearing on healing outcomes. Such critical process is subject to refined control by a multitude of factors, including cytokines, chemokines, and lipid mediators (6). Previous work by our laboratory demonstrated that under conditions of diabetes, resolution of wound inflammation is challenged by several barriers (7). For example, diabetic wounds suffer from impaired engulfment of apoptotic cells by macrophages (mϕ), resulting in increased apoptotic cell burden at the wound site. As a result, resolution of wound inflammation is derailed, complicating healing outcomes (7).

Mϕ are major contributors to cutaneous wound healing (8, 9). At the wound site, successful efferocytosis by mϕ achieves cleansing and resolution of inflammation (10–13). Milk fat globule-epidermal growth factor-factor VIII (MFG-E8) is a secreted glycoprotein that promotes efferocytosis by bridging apoptotic cells with mϕ (14, 15). MFG-E8 contains two epidermal growth factor domains, a proline/threonine-rich domain, and two factor-VIII-homologous domains (15). Mϕ-derived MFG-E8 specifically binds apoptotic cells by recognizing aminophospholipids such as phosphatidylserine (PS). While engaged by PS on apoptotic cells, MFG-E8 binds to dying cells, particularly to integrin $\alpha_v\beta_3$ and $\alpha_v\beta_5$ via its arginine-glycine-aspartate (RGD) motif (15, 16). In addition to its critical role in efferocytosis, MGF-E8 possesses known proangiogenic effect, supporting vascular endothelial growth factor (VEGF) function in adult neovascularization (16). Consistently, recombinant MFG-E8 (rMFG-E8) treatment improves wound angiogenesis (17). However, questions addressing the primary source of MFG-E8 in vivo and the mechanistic underpinnings that determine the significance of MFG-E8 at the wound site remain open. In this work, we sought to characterize the mechanisms by which mϕ-derived MFG-E8 regulates wound inflammation.

Materials and Methods

Human subjects and fluid collection from chronic wounds

Subjects participating in the study were chronic wound patients seen at Ohio State University Comprehensive Wound Center clinics and have been

*Department of Surgery, Ohio State University Wexner Medical Center, Columbus, OH 43210; †Davis Heart and Lung Research Institute, Ohio State University Wexner Medical Center, Columbus, OH 43210; ‡Comprehensive Wound Center, Center for Regenerative Medicine and Cell Based Therapies, Ohio State University Wexner Medical Center, Columbus, OH 43210; §Department of Internal Medicine, Ohio State University Wexner Medical Center, Columbus, OH 43210; and ¶Division of Biosciences, The Ohio State University, Columbus, OH 43210

ORCID: 0000-0002-6927-0266 (J.F.S.).

Received for publication October 23, 2015. Accepted for publication April 18, 2016.

This work was supported by National Institute of Diabetes and Digestive and Kidney Diseases Grant R01 DK076566 (to S.R.), National Institute of Nursing Research Grant NR015676 (to S.R.), National Institute of General Medical Sciences Grants R01 GM069589 and GM077185 (to C.K.S.), and National Institute of Nursing Research Grants NR013898 and NR015676 (to C.K.S.).

The expression data presented in this article have been submitted to the Gene Expression Omnibus (http://www.ncbi.nlm.nih.gov/geo) under accession number GSE73229.

Address correspondence and reprint requests to Dr. Sashwati Roy, 511 Davis Heart and Lung Research Institute, Ohio State University Wexner Medical Center, 473 West 12th Avenue, Columbus, OH 43210. E-mail address: sashwati.roy@osumc.edu

The online version of this article contains supplemental material.

Abbreviations used in this article: AGE, advanced glycation end product; BM, bone marrow; BMDM, BM-derived monocyte; CM, conditioned media; IP, immunoprecipitation; mϕ, macrophage; MerTK, Mer tyrosine kinase; MFG-E8, milk fat globule-epidermal growth factor-factor VIII; MGO, methylglyoxal; NPWT, negative pressure wound therapy; PC, phosphatidylcholine; PS, phosphatidylserine; RGD, arginine-glycine-aspartate; rMFG-E8, recombinant MFG-E8; VEGF, vascular endothelial growth factor.

undergoing negative pressure wound therapy (NPWT) as part of standard clinical care. Demographic characteristics of patients and wound-related information are presented in Table I. The NPWT dressing (sponges) was collected from each patient for cell isolation and wound fluid collection. Wound fluids were derived from NPWT dressing by lavaging the wound dressing with saline solution (18). All human studies were approved by the Ohio State University Institutional Review Board. Declaration of Helsinki protocols was followed, and patients gave their written informed consent.

Secondary intention excisional murine dermal wound model

Male C57BL/6 mice (age 8–10 wk old) were obtained from Harlan Laboratory. Mice homozygous for spontaneous mutation of the leptin receptor ($Lepr^{db}$) (BKS.Cg-$m^{+/+}$ $Lepr^{db/J}$ or db/db; stock 000642) and their respective nondiabetic lean control littermates (db/+) were procured from The Jackson Laboratory. B6.129(Cg)-$Gt(ROSA)26Sor^{tm4(ACTB-tdTomato,-EGFP)Luo}$/J mice obtained from The Jackson Laboratory were bred with LysMcre to produce B6.129(Cg)-$Gt(ROSA)26Sor^{tm4(ACTB-tdTomato,-EGFP)Luo}$/J/LysMcre (ROSA-LysM) mice. The $ROSA^{mT/mG}$ allele is a Cre reporter that expresses cell membrane–targeted two-color fluorescence. In these mice, prior to Cre recombinase exposure, most cells/tissues express red fluorescence. After the exposure to Cre recombinase, the target cells and future cell lineages derived from these cells express membrane-localized green fluorescence protein. Therefore, when bred with LysMcre animals, all cells of myeloid origin express GFP. The MFG-E8 wild-type (MFG-$E8^{+/+}$) and MFG-E8-knockout (MFG-$E8^{-/-}$) mice were provided by S. Nagata (Osaka University Medical School). In brief, the embryonic stem clones harboring the MFG-E8–deficient allele were injected to the host embryos to produce chimeric mice. The resultant chimeric mice were bred with C57BL/6 mice to produce MFG-$E8^{+/-}$ mice. The MFG-$E8^{+/-}$ mice were backcrossed with C57BL/6 for 12 generations, which in turn were bred to generate the MFG-$E8^{+/+}$ and MFG-$E8^{-/-}$ littermates (19). A splinted full-thickness excisional wound model was employed, as described previously (7, 20, 21). Briefly, the dorsal side of the mice was naired and cleaned using betadine under anesthesia. Two 6-mm–diameter full-thickness (skin and panniculus carnosus) excisional wounds were made on the dorsal skin with a 6-mm disposable biopsy punch (22, 23). A donut-shaped splint with an 8-mm inner diameter was made from an 0.5-mm–thick silicone sheet (Grace Bio-Laboratories, Bend, OR) and placed on the wound using an immediate-bonding adhesive, followed by interrupted 5-0 nylon sutures (Ethicon, Somerville, NJ), such that the wound was centered within the splint (7, 22). The wound was covered with semiocclusive dressing (Tegaderm; 3M, St. Paul, MN). For effective topical mouse rMFG-E8 (R&D Systems, Minneapolis, MN) application, the protein solution was injected under the Tegaderm. This approach has effectively delivered recombinant protein delivery to mice excisional wounds (23). Wound imaging was performed at specified times using a digital camera, and the wound area was determined using Image J software (20). The animals were euthanized at specific times, and wound tissues were harvested for molecular and histological analysis. All of the animal studies were performed in accordance with protocols approved by the Laboratory Animal Care and Use Committee of the Ohio State University.

Isolation of murine wound mϕ and BMDM

For wound mϕ, circular (8 mm) sterile polyvinyl alcohol sponges were implanted s.c. on the backs of 8- to 12-wk-old mice (7). Sponge-infiltrated wound mϕ were isolated, as previously described (7, 23). Bone marrow (BM)-derived monocytes (BMDM) were isolated, as previously described (23). Briefly, the femurs of mice (8–12 wk old) were flushed using RPMI 1640, followed by positive selection of the flushed cells using magnetic bead–conjugated CD11b Ab. The isolated day 0 CD11b-positive BMDMs were used for experiments.

Table I. Demographics characteristics of subjects used for wound fluid study

Parameter	Nondiabetic	Diabetic
Subjects (*n*)	5	5
Age	49.6 ± 7.2	48.8 ± 1.2
Males	4	3
Females	1	2
Race		
Caucasian	4	3
African American	1	2
Wound etiology		
Pressure	2	3
Surgical	3	1
Unknown	0	1
Wound location		
Abdominal	1	1
Lower extremity	4	4

Hunt–Schilling wire mesh cylinder for wound fluid collection

Wire mesh cylinders (stainless steel; 2.5 cm length and 0.8 cm diameter) were implanted and wound fluid was harvested, as described previously (24). Briefly, following anesthesia, midline incision (1 cm or smaller) was made on shaved skin with a scalpel. Two small s.c. pockets were created by blunt dissection on either sides of the midline in which wire mesh stainless steel cylinders were implanted. The incisions were closed using sutures. Wound fluid was collected at day 3 postimplantation.

BM chimera

BM chimera was performed, as previously described (25). For establishing chimerism, BM recipient male mice (6–8 wk old) were injected i.p. with busulfan in a 1:1 solution of DMSO and deionized water (30 mg/kg/100 μl) once daily for consecutive 2 d, resulting in partial ablation of the BM. Whole body irradiation, resulting in myeloablation for BM transplantation, is known to result in systemic toxicities (26). Moreover, irradiation is also expected to result in late side effects such as inflammation in skin (27). To circumvent these issues, we chose to use a myelosuppressive approach for partial BM ablation using busulfan, which is an emergent solution that is being widely embraced, depending on the specific questions addressed in a given study (25, 28, 29). In our case, it was important to avoid the above-mentioned confounding factors that come with whole body irradiation. Donor BM-derived cells isolated from the femur were injected into recipient mice by tail vein injection (100 μl) 48 h after the second dose of busulfan. Donor BM-derived cells were obtained from C57BL/6-Tg (CAG-EGFP), MFG-$E8^{+/+}$, or MFG-$E8^{-/-}$ mice. Following BM transfer, mice were left undisturbed for 4 wk to allow engraftment, which was ascertained by determining the presence of GFP cells in the BM and the blood.

Apoptotic cell clearance assay

Apoptotic cell clearance assay (efferocytosis) was performed, as previously described (7). Briefly, wound mϕ were cocultured in eight-well chambered slides with apoptotic (5 μM dexamethasone treated for 12 h; yield >90% PS-positive thymocytes) thymocytes (labeled with pHrodo succinimidyl ester; Invitrogen) in 1:10 mϕ:thymocyte ratio. Efferocytosis studies were performed using cultured mϕ ex vivo for 1 h at 37°C, followed by extensive washes to remove nonengulfed cells. Cells were then fixed with 4% paraformaldehyde and stained using F4/80-FITC, followed by imaging using a fluorescence microscope. Efferocytosis index was calculated as the total number of engulfed apoptotic cells per mϕ present in the field of view (7, 30, 31).

GeneChip probe array analyses

RNA extraction, target labeling, GeneChip, and data analysis were performed, as described previously (21, 32). Briefly, in vitro transcription reaction was performed using GeneChip IVT Labeling Kit (Affymetrix, Santa Clara, CA) to generate biotinylated cRNA from RNA samples. The samples were hybridized to Affymetrix Mouse Genome U133 Plus 2.0 Array. The arrays were washed, stained with streptavidin-PE, and scanned with the GeneArray scanner (Affymetrix) in our own facilities, as described earlier (21, 32). Gene Chip Operating Software (Affymetrix) was employed for data acquisition and image processing. The expression data have been submitted to the Gene Expression Omnibus (http://www.ncbi.nlm.nih.gov/geo) with the series accession number GSE73229. Raw data were analyzed using Genespring GX (Agilent, Santa Clara, CA). Additional processing of data was performed using dChip software (Harvard University, Cambridge, MA) (21, 32).

Immunohistochemistry

Immunostaining of CD31 and MFG-E8 was performed on cryosections of wound tissue samples using specific Abs, as described previously (22, 33). Briefly, 10-μm–thick cryosectioned tissues were fixed with cold acetone, blocked with 10% normal goat serum, and incubated with specific Abs against CD31 (BD Pharmingen; 1:400) and MFG-E8 (MBL International; 1:100) overnight at 4°C. Signal was visualized by subsequent incubation with fluorescence-tagged secondary Abs (Alexa 568–tagged α-rat, 1:200; Alexa 405–tagged α-hamster, 1:200), followed by counterstaining with DAPI. Images were captured by microscope, and quantification of fluorescent intensity of image was performed using AxioVision Rel 4.6 (Carl Zeiss Microimaging) software. Colocalization of immunostains was performed using FV10-ASW software from Olympus.

ELISA

Levels of MFG-E8, TNF-α, and IL-10 (R&D Systems, Minneapolis, MN) were measured using commercially available ELISA kits (23, 31). The serum levels of MFG-E8 in murine wound fluid were measured using ELISA, as described (34). In brief, PS solution in methanol was coated onto 96-well plates, followed by blocking the wells with BSA (10 mg/ml). The serum was added to the wells and incubated at room temperature for 2 h, followed by washing with PBS containing 0.05% Tween 20. The MFG-E8 bound to the wells was detected using anti–MFG-E8 (mouse) mAb (MBL; clone 18A2-G10) and HRP-linked anti-hamster secondary Ab. The levels of MFG-E8 in wound fluid were normalized against albumin concentration in the fluid (23). Albumin levels were determined by ELISA (AssayPro, St. Charles, MO) (23).

RNA extraction, reverse transcription, and quantitative RT-PCR

mirVana RNA isolation kit (Ambion, Austin, TX) was used, according to the manufacturer's instructions, to extract total RNA, as previously described (18). Quantification of mRNA was done by real-time or quantitative PCR assay using dsDNA binding dye SYBR Green-I, as described previously (21, 32, 35).

Matrigel assay

In vitro angiogenesis assay was assessed by tube formation ability on Matrigel culture, as described previously (22, 33, 36). Murine dermal endothelial cells (Cell Biologics) were seeded on Matrigel (Cultrex basement membrane extract reduced growth factor; R&D Systems, Minneapolis, MN)-precoated four-well plates at a density of 8×10^4 cells/well. The angiogenic ability of 24-h cell supernatants (conditioned media [CM]) from day 7 wound mϕ (treated with/without rMFG-E8 and recombinant VEGF; R&D Systems) of MFG-E8$^{+/+}$ WT and MFG-E8$^{-/-}$ mice was assessed 8 h after plating on Matrigel, followed by staining with 3 μM calcein-AM (Invitrogen) for 20–30 min at 37°C and 5% CO_2, as previously described (37). The tube length was measured using the software AxioVision Rel 4.6 (Zeiss) (20, 22).

Western blot

Western blot was performed using primary Ab against MFG-E8 (MBL International), phospho- Mer tyrosine kinase (MerTK; FabGennix; 1:750), and active caspase 3 (Cell Signaling), as described previously (24, 31, 38). Signal was visualized using corresponding HRP-conjugated secondary Ab (Amersham; 1:3000) and ECL Plus Western blotting detection reagents (Amersham). β-actin (Sigma-Aldrich; 1:5000) served as loading control.

Wound vascularity and blood flow

Wound vascularity. Prior to sacrifice of mice, space-filling carboxylate-modified fluorescent microspheres (FluoSpheres, 0.2 μm, 1012 particles/ml) were injected into the left ventricle of the beating heart, as previously described (24, 39).

Laser speckle. Dermal blood flow was analyzed by laser speckle imager, as described previously (40). The mean blood flow was measured in excisional wounds using PeriCam PSI System within a 100-mm^2 surface area (resolution 0.54 × 0.54 mm, working distance 10–20 cm).

Immunoprecipitation

Immunoprecipitation (IP) of MFG-E8 was done, as previously described (41, 42). Wound-edge tissue lysates (100 μg) of diabetic animals were incubated with 5 μg MFG-E8 mAb (clone 2422) overnight in a rotisserie shaker at 4°C. Protein A-agarose beads (Invitrogen) were prewashed with lysis buffer (150 mM KCl, 25 mM Tris-HCl, 5 mM EDTA, 0.5% IgePal, 1 mM PMSF, protease inhibitor) and incubated with the lysate–Ab mix for 3 h at 4°C to immunoprecipitate MFG-E8. The beads were then washed three times with ice-cold lysis buffer, and the immunoprecipitated complexes were washed four times with lysis buffer. For Western blot, the IP samples were subjected to SDS-PAGE after reduction with 1 M DTT, as previously described (37, 41), and probed with anti-AGE Ab (1:1000 dilution; Abcam). The membrane was stripped and reprobed with anti–MFG-E8 Ab (clone 18A2-G10).

MFG-E8 glycation and surface-plasmon resonance analysis (Biacore)

For glycation of MFG-E8, 50 μg mouse rMFG-E8 (R&D Systems) was treated with 10 mM methylglyoxal (MGO; Sigma-Aldrich) at 37°C. To obtain dose-dependent glycation, the reaction with MGO was performed for specific durations (0, 3, and 48 h). The glycation of MFG-E8 was determined using Pierce Glycoprotein Carbohydrate Estimation kit (Pierce). The binding affinity of MFG-E8 and glyacted MFG-E8 to PS was analyzed on Sensor chip L1 (GE Healthcare Life Sciences) using Biacore T100 (43, 44).

Data collection and statistical analyses

For in vitro experiments, data are reported as mean ± SD of three to six experiments, as indicated in respective figure legends. For animal studies,

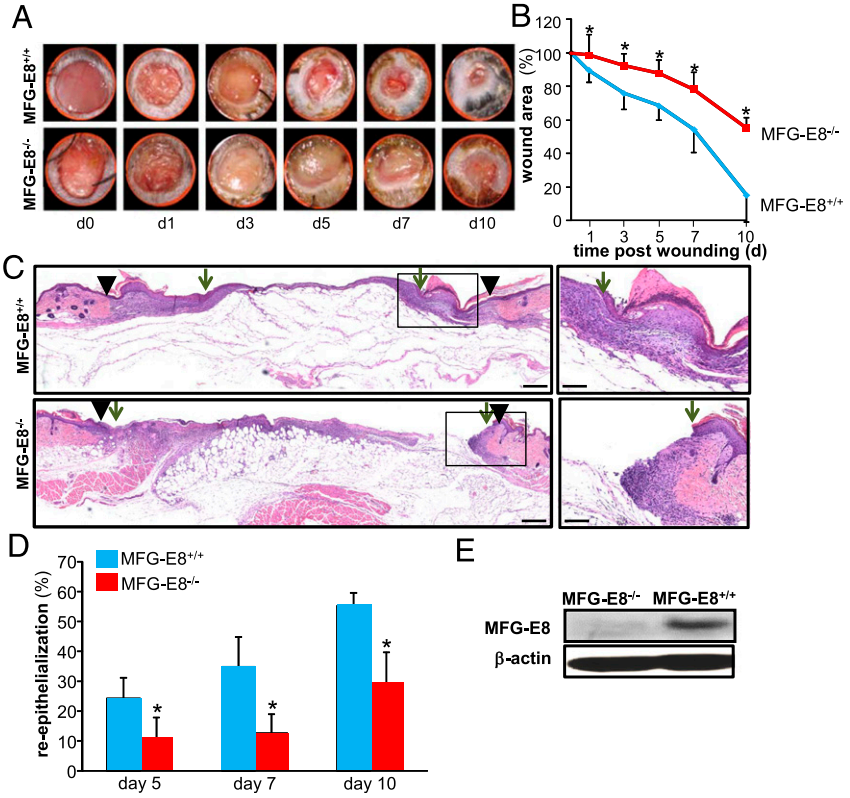

FIGURE 1. MFG-E8 deficiency impairs wound closure and wound re-epithelialization. (**A**–**D**) Full-thickness (skin and panniculus carnosum) dorsal wounds were created on the male MFG-E8$^{-/-}$ and MFG-E8$^{+/+}$ mice by using a 6-mm biopsy punch. The wounds were stented and left to heal by secondary intention. Wounds were imaged on day 0–10 postwounding. Wound areas were calculated using digital planimetry. (A) Representative digital images of wounds from age-matched MFG-E8$^{-/-}$ and MFG-E8$^{+/+}$ mice day 0–10 postwounding. (B) Wound closure kinetics. Data are expressed as mean ± SD (n = 5). *$p < 0.05$ compared with MFG-E8$^{+/+}$ wounds. (C) Representative images of H&E-stained day 7 wound tissues. The wound edge is shown using solid black arrowheads, and the wound epithelial margins are shown by green arrows. Scale bar, 330 μm. The *right panel* shows the zoomed image of the *inset* (scale bar, 100 μm). (D) Wound re-epithelialization calculated on day 5, 7, and 10 postwounding. Data are expressed as mean ± SD (n = 3). *$p < 0.05$ compared with MFG-E8$^{+/+}$ wounds. (**E**) Western blot analysis of MFG-E8-L protein expression in skin from MFG-E8$^{+/+}$ and MFG-E8$^{-/-}$ mice. β-actin was used as a loading control.

data are reported as mean ± SD of at least three to eight animals, as indicated. For human wound fluid studies, data from human subjects ($n = 10$) have been presented (Table I). Student t test (two tailed) was used to determine significant differences. Comparisons among multiple groups were tested using ANOVA. A p value <0.05 was considered statistically significant.

Results

MFG-E8 deficiency impairs wound closure and wound re-epithelialization

MFG-E8$^{-/-}$ and age-matched MFG-E8$^{+/+}$ mice were used to test the significance of MFG-E8 in wound healing. MFG-E8$^{-/-}$ mice exhibited significantly delayed wound closure kinetics as compared with the wild-type age-matched littermates. By day 10, when ~90% of the wounds of the wild-type animals were fully closed, the wounds of null mice were still 60% open (Fig. 1A, 1B). Wound re-epithelialization was significantly impaired on day 5–10 postwounding in null mice as compared with the wild-type animals (Fig. 1C, 1D). Loss of MFG-E8 protein in the skin of null mice was confirmed by Western blot (Fig. 1E).

Expressed by wound-site macrophages, MFG-E8 supports efferocytosis and resolves wound inflammation

Wound-edge tissues were collected on day 3, 5, 7, and 10 postwounding to study the abundance of MFG-E8. A significant increase in wound-edge MFG-E8 protein was noted on day 3 and 5 postwounding (Fig. 2A). To determine whether MFG-E8 is induced in wound mϕ, MFG-E8 expression in wound mϕ was compared with monocytes derived from BM (BMDM). Although MFG-E8 was almost undetectable in BMDM, MFG-E8 in day 3 wound mϕ was abundant (Fig. 2B). MFG-E8-L form and not the -S form has been shown to serve as a linker between phagocytic cells and apoptotic cells (15). The -L form is produced by macrophages (15) and was found to be predominantly expressed in the skin using a MFG-E8 Ab raised in hamster (MBL; clone 18A2-G10) (Fig. 2A).

The cells/tissue of B6.129(Cg)-Gt(ROSA)26Sor$^{tm4(ACTB-tdTomato,-EGFP)Luo}$/J/LysMcre (ROSA-LysM) mice widely express cell membrane-localized red fluorescence. However, because of LysM-driven cre-recombinase, only the cells of myeloid origin express membrane-localized green fluorescence. Expectedly, the wound mϕ (GFP$^+$, green) abundance at the wound site peaked on day 3 and 5 postwounding (Fig. 2C). Using these ROSA-LysM mice, we investigated the significance of mϕ as a source of MFG-E8 in wounds. The increase of wound-site MFG-E8 levels was coincident with the kinetics of mϕ recruitment to the site (Fig. 2C, Supplemental Fig. 1). Immunohistochemical staining of MFG-E8 in day 3 wound-edge tissue of ROSA-LysM mice showed that 65% of wound-site MFG-E8 signal was colocalized with wound (Fig. 2D). Taken together, these data reveal that during the inflammatory phase (day 3–5 postwounding), wound mϕ are a major source of MFG-E8 at the wound site (Fig. 2B–D).

MFG-E8 serves as a bridging molecule between apoptotic cells and phagocytes enabling efferocytosis (15). Wound mϕ from

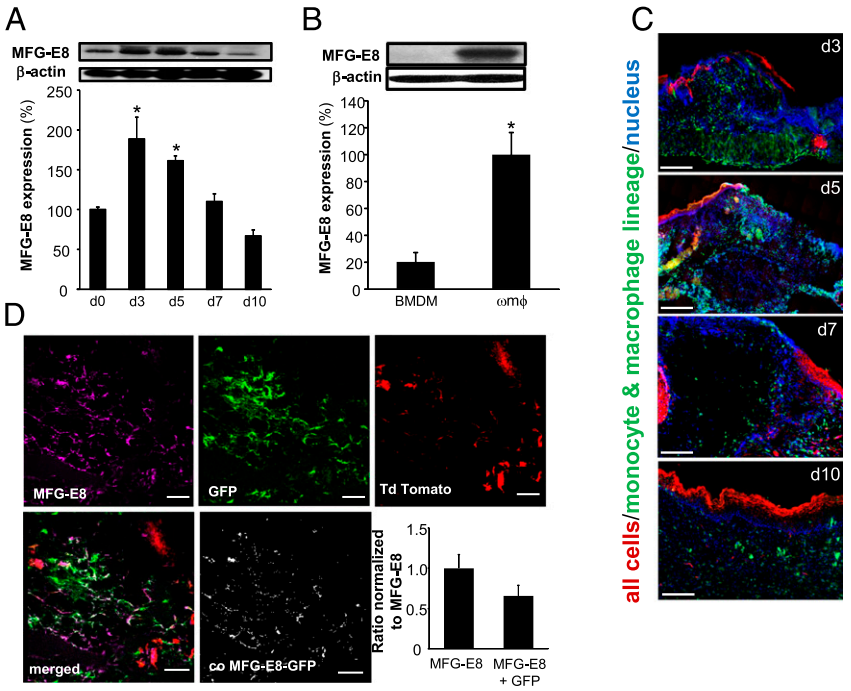

FIGURE 2. Macrophages are the primary source of MFG-E8 at wound site in inflammatory phase. (**A**) Western blot analysis of MFG-E8 protein expression in wound-edge tissues from C57BL/6 mice on day 0–10 postwounding. β-actin was used as loading control. Representative blot from four independent experiments has been provided. Densitometry quantification of the Western blot data was performed. Data are presented as percentage of change compared with day 0 (skin). Data are expressed as mean ± SD ($n = 4$). *$p < 0.05$ compared with day 0 (skin). (**B**) Western blot analysis of MFG-E8 protein expression in BMDM and day 3 wound mϕ (ωmϕ). β-actin was used as a loading control. Representative blot from three independent experiments has been provided. Densitometry quantification of Western blot data has been presented. Data are expressed as mean ± SD ($n = 3$). *$p < 0.05$ as compared with BMDM. (**C**) Representative images of wound-edge tissue sections day 3–10 postwounding from ROSA-LysM mice displaying abundance of wound mϕ (GFP$^+$, green) at the wound site peaked on day 3 and 5 postwounding. Most cells/tissue in these mice widely express cell membrane–localized red fluorescence; however, because of LysM-driven cre recombinase, only the cells of myeloid origin express membrane-localized green fluorescence. DAPI (blue, nuclear) staining was performed on wound tissue sections, followed by fluorescence microscopy and imaging. Scale bar, 500 μm. (**D**) Representative images of day 3 wound-edge tissue sections from ROSA-LysM mice stained with MFG-E8 (purple, pseudocolor) to observe colocalization of MFG-E8 with green wound mϕ. The bar graph represents the ratio of MFG-E8 that is contributed by macrophages (MFG-E8 colocalized with GFP-positive macrophages) to the total MFG-E8 (purple) in field of view. The ratio of purple:green colocalization in confocal images was determined using automated unbiased colocalization module in FV10-ASW software (Olympus). Scale bar, 50 μm. Bar graph represents the fraction of MFG-E8 that is contributed by macrophages.

MFG-E8$^{-/-}$ mice exhibited significantly compromised efferocytosis activity compared with those from the wild-type animals (Fig. 3A, 3B). Successful efferocytosis is known to suppress proinflammatory and upregulate anti-inflammatory genes (30, 45). Inducible NO synthase and arginase are classical markers for M1 and M2 macrophages, respectively (46). Consistently, nonefferocytosing mϕ from MFG-E8$^{-/-}$ mice showed a proinflammatory M1 phenotype featuring high proinflammatory inducible NO synthase and low anti-inflammatory arginase (Supplemental Fig. 2).

MerTK, a member of the Axl/Mer/Tyro3 receptor tyrosine kinase family, is required for efferocytosis by mϕ (47). The phosphorylation of MerTK was determined as an additional evidence of impaired efferocytosis in MFG-E8$^{-/-}$. Postefferocytotic wound mϕ from MFG-E8$^{-/-}$ mice exhibited lower MerTK phosphorylation (Fig. 3C). Efferocytosis is known to cause MerTK phosphorylation (48–50). This is consistent with our observation that impaired efferocytosis (Fig. 3A, 3B) in MFG-E8$^{-/-}$ mice blunted MerTK phosphorylation postefferocytosis. Apoptotic cell burden at the wound-edge tissue was measured by immunoblotting active caspase 3. The day 7 wound-edge tissue from MFG-E8$^{-/-}$ exhibited significantly higher active caspase-3 levels as compared with wild-type wound tissues indicating higher apoptotic cell burden (Fig. 3D).

Our laboratory has reported that increasing apoptotic cell burden at wound site results in prolonged inflammatory response (7). Consistently, wound edge of MFG-E8$^{-/-}$ that were burdened with apoptotic cells displayed a proinflammatory phenotype as exemplified by augmented levels of proinflammatory TNF-α (Fig. 3E) and decreased levels of anti-inflammatory IL-10 (Fig. 3F).

Impaired wound angiogenesis in MFG-E8$^{-/-}$ mice

Timely resolution of wound inflammation is a prerequisite for the onset of wound angiogenesis (51, 52). To elucidate the molecular mechanisms by which MFG-E8 supports wound healing, unbiased transcriptome profiling of wound-edge tissue (day 5 postwounding) from MFG-E8$^{-/-}$ and control MFG-E8$^{+/+}$ mice was performed. Pathway analysis identified a distinct cluster of proangiogenic genes that were potently downregulated in the wound edge of MFG-E8$^{-/-}$ animals (Fig. 4A, 4B). These data were further validated using quantitative RT-PCR (Fig. 4C). Findings of transcriptome analysis were extended to examine whether indeed the wounds of MFG-E8$^{-/-}$ mice display impaired angiogenesis. Decreased abundance of wound-edge CD31^{+} endothelial cells was noted in the MFG-E8$^{-/-}$ mice (Fig. 4D, Supplemental Fig. 3). Wound vascularization was further monitored using fluorescent microspheres (0.2 μm; fluoSpheres carboxylate-modified microspheres, green fluorescent; Molecular Probes) that were injected into the left ventricle (53) (Fig. 4E, Supplemental Fig. 3). A marked decrease in the number of green microspheres at the wound site of MFG-E8$^{-/-}$ mice demonstrated compromised wound angiogenesis. Finally, the functional analysis of blood flow at the wound site performed using laser speckle perfusion imaging demonstrated a marked decrease in blood flow in MFG-E8$^{-/-}$ mice (Fig. 4F). These data collectively establish that at the wound site MFG-E8 plays a critical role in supporting wound angiogenesis.

Wound macrophage-derived MFG-E8 is angiogenic

To test the angiogenic potential of mϕ-derived MFG-E8, Matrigel tube formation was performed using CM from day 7 wound mϕ of

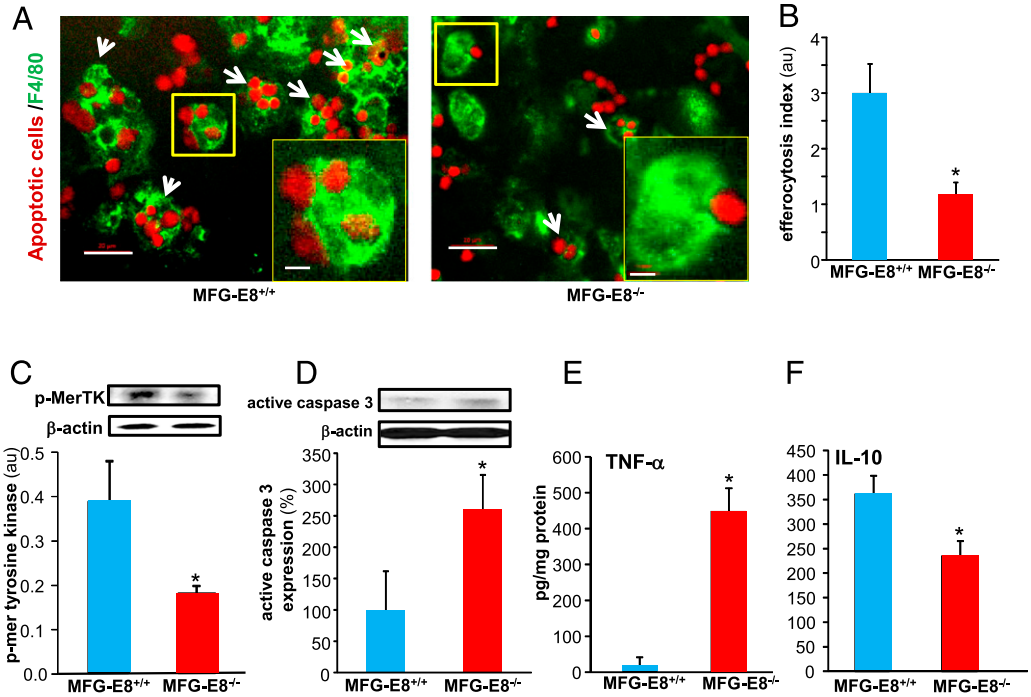

FIGURE 3. MFG-E8 supports efferocytosis and resolves inflammation at the wound site. (**A** and **B**) Efferocytosis activity in wound mϕ harvested from MFG-E8$^{-/-}$ and MFG-E8$^{+/+}$ mice. (A) Representative images of wound mϕ (F4/80, green) cocultured with apoptotic cells (pHrodo, red). White arrows point to mϕ that have engulfed two or more apoptotic cells. Scale bar, 20 μm. *Inset*, Zoom of yellow box in the image showing single mϕ engulfed apoptotic cells. Scale bar, 5 μm. (B) Efferocytosis index in day 3 wound mϕ. Efferocytosis index is defined as the total number of engulfed apoptotic cells per mϕ present in a field of view. Data are expressed as mean ± SD (n = 3). *$p < 0.05$ compared with MFG-E8$^{+/+}$ group. (**C** and **D**) Western blot of (C) MerTK phosphorylation in day 3 wound mϕ following efferocytosis. (D) Active caspase 3 expression in day 7 wound-edge tissues. β-actin was used as a loading control. Representative blot from four independent experiments has been provided. Densitometry quantification of band intensity has been presented. Data are expressed as mean ± SD (n = 4). *$p < 0.05$ compared with MFG-E8$^{+/+}$ wound mϕ and wound-edge tissues, respectively. (**E** and **F**) Quantification of (E) TNF-α and (F) IL-10 measured by ELISA in the day 7 wound-edge tissues. Data are expressed as mean ± SD (n = 4). *$p < 0.05$ compared with MFG-E8$^{+/+}$ wounds.

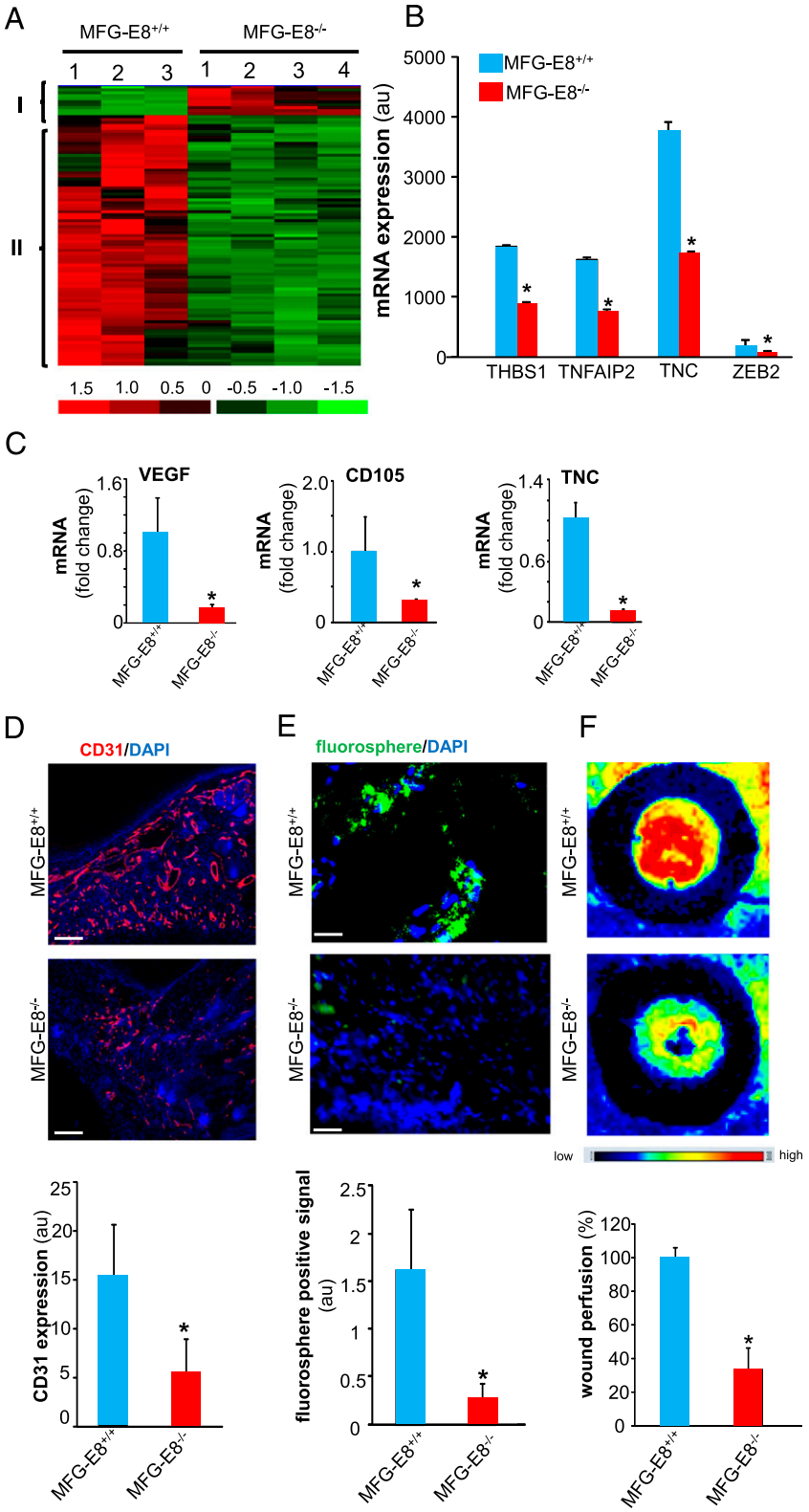

FIGURE 4. Impaired wound angiogenesis in MFG-E8$^{-/-}$ mice. (**A**) All MFG-E8–sensitive transcripts in day 5 wound-edge tissues were subjected to hierarchical clustering. (A) Two major clusters of transcripts that were differentially ($p <$ 0.05, 2-fold or higher) regulated in MFG-E8$^{-/-}$ as compared with corresponding wild-type (MFG-E8$^{+/+}$) were identified. Red to green gradation in color represents higher to lower expression signal. A scale representing fold change is indicated at the bottom. (**B**) Fold change of representative proangiogenic genes from microarray analysis has been presented. Data are expressed as mean ± SD (n = 3). *$p < 0.05$ compared with MFG-E8$^{+/+}$ wound-edge tissues. (**C**) Expression levels of selected genes identified using GeneChip analyses were independently determined using real-time quantitative PCR. Data are expressed as mean ± SD (n = 3). *$p < 0.05$ compared with MFG-E8$^{+/+}$ wound-edge tissues. (**D**) Representative images from CD31 (red) immunostained day 5 wound-edge sections. The sections were counterstained with DAPI (blue, nuclear). Bar graph presents the quantification of CD31-positive areas of the day 5 wound-edge tissues. Results are mean ± SD (n = 3). *$p < 0.05$ compared with MFG-E8$^{+/+}$ wounds. Scale bar, 200 μm. (**E**) Representative images from space-filling carboxylate-modified green fluorescent microsphere-injected mice to visualize wound vascularity. Sections were counterstained with DAPI (blue, nuclear). The appearance of the green microspheres in the wound edge represents functional wound vascularity. Results are mean ± SD (n = 4). *$p < 0.05$ compared with MFG-E8$^{+/+}$ wound-edge tissues. Scale bar, 200 μm. (**F**) Laser speckle images of day 5 wounds. Bar graph represents the quantitative data from laser speckle analysis. Data presented as mean ± SD (n = 4). *$p < 0.05$ compared with MFG-E8$^{+/+}$ wounds.

MFG-E8$^{-/-}$ and MFG-E8$^{+/+}$ mice. Tube formation of murine dermal endothelial cells was significantly better when incubated with CM from MFG-E8$^{+/+}$ mϕ compared with that in response to CM from MFG-E8$^{-/-}$ mϕ. Impairment of such tube formation in response to CM from MFG-E8$^{-/-}$ mϕ was partially rescued by replenishing the CM with rMFG-E8. Adding both rMFG-E8 and recombinant VEGF to the CM fully restored Matrigel angiogenic response (Fig. 5A, 5B). Furthermore, the expression of major angiogenic genes was significantly downregulated in the wound mϕ of MFG-E8$^{-/-}$ mice (Fig. 5C–E). Thus, in wound mϕ, MFG-E8 is angiogenic.

To further test the significance of mϕ-derived MFG-E8 on wound angiogenesis and healing, BM transplantation was performed involving ablation of the BM by busulphan injection, followed by reconstitution using the donor BM (Supplemental Fig. 4). Transplantation of MFG-E8$^{-/-}$ BM to MFG-E8$^{+/+}$ mice

resulted in impaired wound closure (Fig. 6A, 6B) and compromised wound vascularization (Fig. 6C, 6D) compared with the MFG-E8$^{+/+}$ mice receiving wild-type BM. In contrast, MFG-E8$^{-/-}$ mice that received wild-type BM showed improved wound closure (Fig. 6E, 6F) and improved wound vascularization (Fig. 6G, 6H). This line of evidence firmly establishes a significant angiogenic role wound mϕ-derived MFG-E8.

Lower MFG-E8 levels in the diabetic wound environment

MFG-E8 protein levels were determined in wound fluids obtained from patients with chronic wounds. The MFG-E8 level was significantly lower in the wound fluid from chronic wound patients with clinically diagnosed diabetes as compared with the fluids obtained from chronic wound patients without diabetes (Fig. 7A). Patient demographic is listed in Table I. Consistent data were obtained in the wound fluids from diabetic mice (Lepr^{db}, db/db) as compared with age-matched nondiabetic controls (heterozygous, Lepr$^{db/+}$, m+/db) (Fig. 7B). It is known that under diabetic conditions, hyperglycemia may cause nonenzymatic glycation of free amino groups of proteins that then leads to the structural and functional changes in these proteins. Such changes may mask immunodetection of MFG-E8, rich in RGD and proline/threonine-rich domains.

To determine whether MFG-E8 is glycated in diabetic wounds, IP of MFG-E8 from diabetic wounds followed by cross blotting with anti-AGE Ab was performed. The data indicate that MFG-E8 in diabetic ulcers gets glycated (Fig. 7C). We tested whether the binding affinity of MFG-E8 to PS is compromised following glycation of MFG-E8. Such binding affinity was tested using surface plasmon resonance (Biacore) with PS or phosphatidylcholine (PC) (as a reference) liposomes immobilized on the sensor chip and glycated MFG-E8 or native MFG-E8 as soluble analytes. MFG-E8 exhibited preferential binding with PC:PS (50:50 mol/mol) as compared with PC:PS (100:0 mol/mol). Glycated MFG-E8 displayed weak binding affinity to PS as compared with the binding of sham with PS (Fig. 7D–F). To obtain dose-dependent glycation, the reaction with MGO was performed for specific durations (0, 3, and 48 h). Such incubation resulted in significant differences in glycation of MFG-E8 at 3 and 48 h (Fig. 7H). The dose-dependent glycation of MFG-E8 resulted in dose-dependent inactivation of MFG-E8 toward binding to PS, as measured using Biacore (Fig. 7G). Thus, MFG-E8 is subject to glycemic modification resulting in loss of PS-binding activity, which in turn blunts efferocytosis.

MFG-E8 treatment improves efferocytosis, angiogenesis, and healing in diabetic wounds

The treatment of isolated diabetic wound mϕ with MFG-E8 improved efferocytosis activity (Fig. 8A). Topical treatment of diabetic wounds with rMFG-E8 (1 μg each wound daily once) favored resolution of inflammation by lowering TNF-α levels and increasing anti-inflammatory IL-10 levels at the wound-edge tissue (Fig. 8B). Resolution of inflammation is known to favor the wound angiogenesis cascade. Consistently, topical treatment of diabetic wounds with rMFG-E8 markedly improved wound angiogenesis (Fig. 8C). These favorable effects of topical rMFG-E8 were eventually recorded as faster wound closure (Fig. 8D, 8E).

Discussion

MFG-E8 is a peripheral glycoprotein that acts as a bridging molecule between the mϕ and apoptotic cells, thus executing a pivotal role in the scavenging of apoptotic cells from affected tissues (15). Expressed and secreted by activated mϕ and dendritic cells, MFG-E8 is versatile and displays a wide array of functions

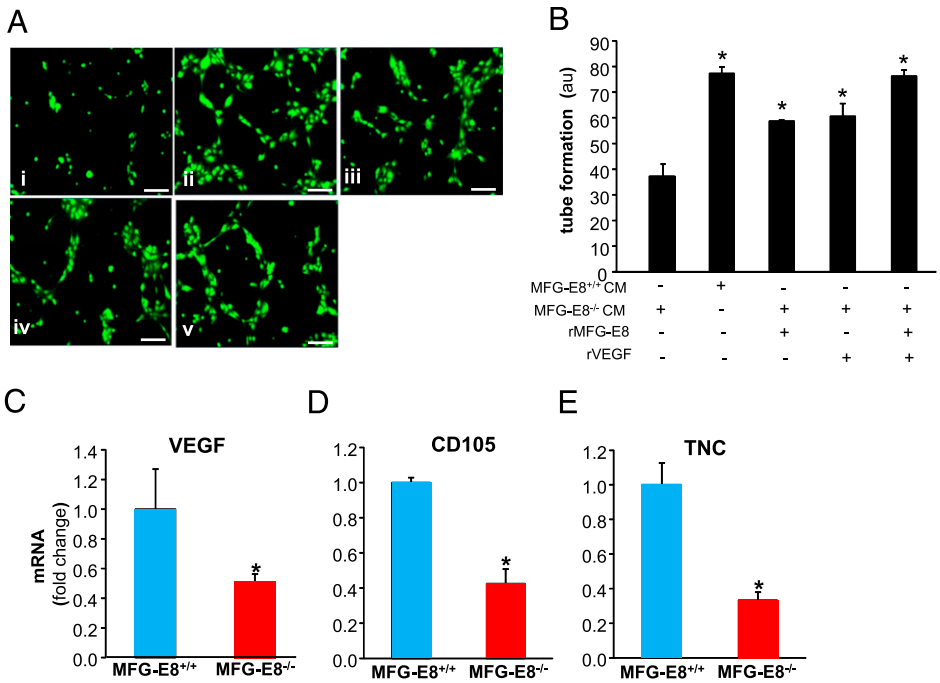

FIGURE 5. Wound macrophage-derived MFG-E8 is angiogenic. (**A**) Representative images of murine dermal endothelial cells subjected to Matrigel assay. Following the assay, calcein-AM (green) was used to stain and visualize the tube formation. The Matrigel assay was performed in presence of CM from day 7 wound mϕ obtained from MFG-E8$^{-/-}$ and MFG-E8$^{+/+}$ mice. The CM was obtained by culturing freshly isolated wound mϕ 24 h in a standard media. (**i**) CM from MFG-E8$^{-/-}$; (**ii**) CM from MFG-E8$^{+/+}$; (**iii**) CM from MFG-E8$^{-/-}$ + rMFG-E8 (2.5 μg); (**iv**) CM from MFG-E8$^{-/-}$ + VEGF (50 ng); or (**v**) CM from MFG-E8$^{-/-}$ + rMFG-E8 (2.5 μg) + VEGF (50 ng). Scale bar, 100 μm. (**B**) Data presented in (A) were quantified and presented as bar graphs. Results are mean ± SD (n = 4). *$p < 0.05$ compared with cells treated with CM from MFG-E8$^{-/-}$ mice. (**C**–**E**) Expression of specific proangiogenic genes (C) VEGF, (D) CD105, and (E) TNC in wound mϕ. The expressions were measured using real-time PCR. Results are mean ± SD (n = 3). *$p < 0.05$ compared with MFG-E8$^{+/+}$ wound mϕ.

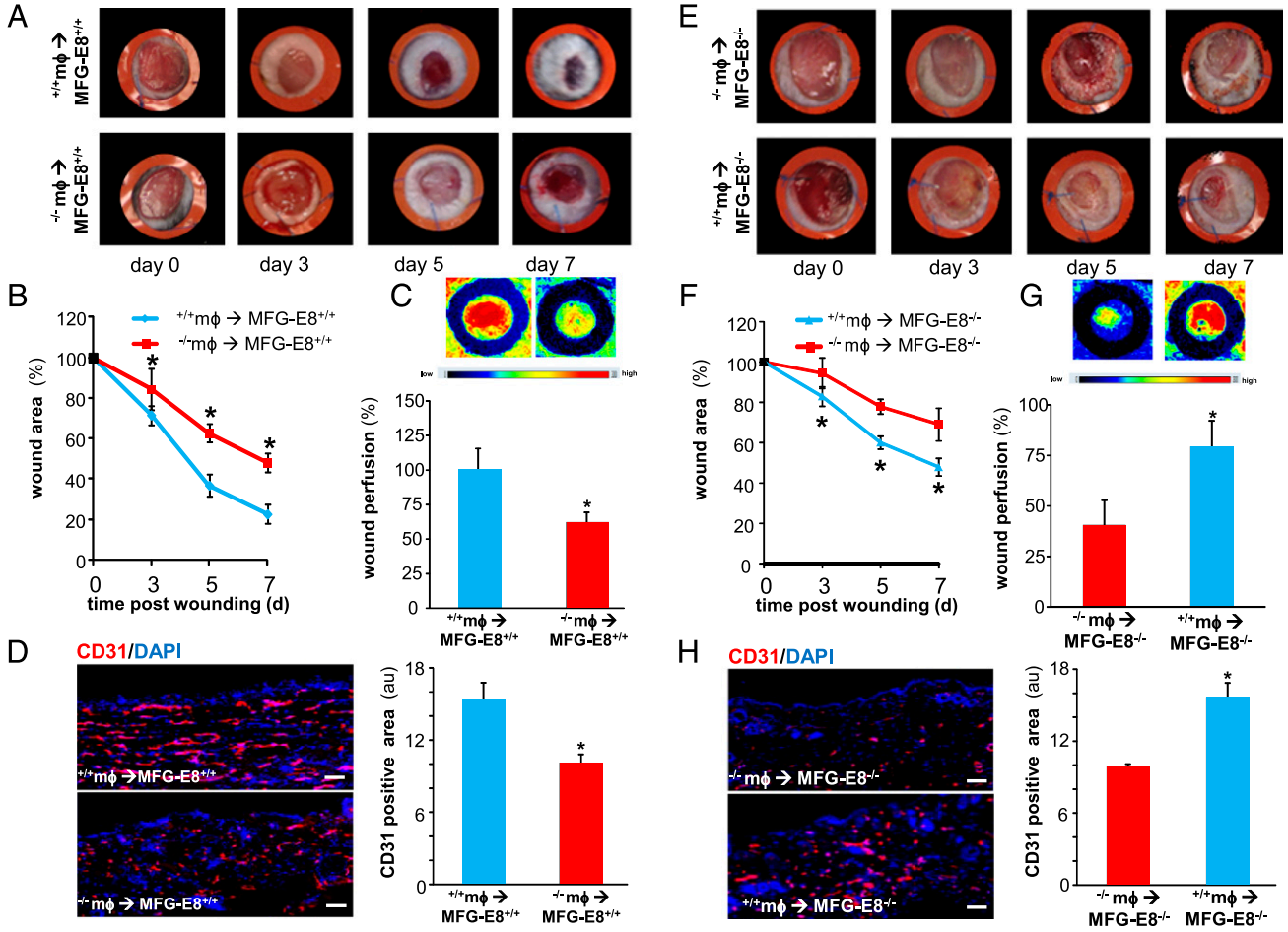

FIGURE 6. Rescuing MFG-E8 levels in the MFG-E8$^{-/-}$ mice wound macrophages using BM transplantation improves wound angiogenesis and closure. BM chimera generation involved ablation of the BM, followed by reconstitution using the donor BM either from MFG-E8$^{+/+}$ or MFG-E8$^{-/-}$ mice. (**A** and **B**) Full-thickness dorsal wounds were created using a 6-mm biopsy punch. The wounds were stented and left to heal by secondary intention. Wounds were imaged on day 0–7 postwounding. (A) Representative digital images of wounds of MFG-E8$^{+/+}$ mice that received MFG-E8$^{-/-}$ mϕ ($^{-/-}$ mϕ→MFG-E8$^{+/+}$) or MFG-E8$^{+/+}$ mice that received MFG-E8$^{+/+}$mϕ ($^{+/+}$mϕ→MFG-E8$^{+/+}$). (B) Wound area measurements using digital planimetry. Data are expressed as mean ± SD ($n = 4$). *$p < 0.05$ as compared with $^{+/+}$mϕ→MFG-E8$^{+/+}$ mice. (**C**) Laser speckle images of day 5 wounds presented in (A) and (B). Bar graph represents the quantitative data from laser speckle analysis. Data presented as mean ± SD ($n = 4$). *$p < 0.05$ compared with $^{+/+}$mϕ→MFG-E8$^{+/+}$ mice. (**D**) CD31 (red) immunostaining was performed in day 5 wound-edge tissues. Bar graph represents the quantification of CD31-positive area. Results are mean ± SD ($n = 4$). *$p < 0.05$ compared with $^{+/+}$mϕ→MFG-E8$^{+/+}$ group. Scale bar, 100 μm. (**E**) Representative digital images of wounds of MFG-E8$^{-/-}$ mice that received MFG-E8$^{+/+}$ mϕ ($^{+/+}$ mϕ→MFG-E8$^{-/-}$) or MFG-E8$^{-/-}$ mice that received MFG-E8$^{-/-}$ mϕ ($^{-/-}$mϕ→MFG-E8$^{-/-}$). (**F**) Wound area measurements using digital planimetry. Data are expressed as mean ± SD ($n = 4$). *$p < 0.05$ as compared with $^{-/-}$mϕ→MFG-E8$^{-/-}$ mice. (**G**) Laser speckle images of day 5 wounds presented in (E) and (F). Bar graph represents the quantitative data from laser speckle analysis. Data presented as mean ± SD ($n = 4$). *$p < 0.05$ compared with $^{-/-}$mϕ→MFG-E8$^{-/-}$ mice. (**H**) CD31 (red) immunostaining was performed in day 5 wound-edge tissues. Bar graph represents the quantification of CD31-positive area. Results are mean ± SD ($n = 4$). *$p < 0.05$ compared with $^{-/-}$mϕ→MFG-E8$^{-/-}$ group. Scale bar, 100 μm.

in cell physiology (15, 54). The therapeutic potential of this multidomain protein has been recognized in a multitude of diseased conditions, such as cancers, sepsis, and ischemia–reperfusion injury of the heart and dextran sulfate sodium–induced colitis (54–56). MFG-E8 has anti-inflammatory properties primarily executed by its effects on mϕ cell biology (57, 58). Nonresolving inflammation is a key factor that underlies chronic wounds such as diabetic ulcers (2). The significance of MFG-E8 in managing wound inflammation is thus of extraordinary interest. The current study recognizes wound mϕ MFG-E8 function as being critical in resolving wound inflammation. Importantly, it upholds an extraordinary significance of MFG-E8 in effectively managing diabetic wound complications.

Wound-site mϕ are key drivers of the healing process (5, 8, 9, 59). The site of injury is laden with dead cells. Timely debridement of apoptotic cells by wound-site mϕ paves the way to the resolution of inflammation (10–13). Under conditions of diabetic complications, such efferocytosis is compromised, resulting in increased apoptotic cell burden at the wound site. Inability of wound-site mϕ to execute efferocytosis results in a persisting proinflammatory milieu that complicates healing outcomes (7). Functionally, MFG-E8 enables efferocytosis by binding to PS on apoptotic cell surface and tethering them to mϕ via integrin receptors. However, the origin of MFG-E8 is contentious and dependent on the context. In tumors, pericytes represent a major source of the secreted MFG-E8 (60). Although direct evidence was limited, inspired by the tumor findings it was speculated that pericytes are the primary source of MFG-E8 at the wound site (17). To our knowledge, the present study is the first to establish mϕ as the primary contributor of MFG-E8 in the inflammatory phase of cutaneous wound healing.

Cutaneous wounds of loose-skinned animals such as mice, unlike humans, primarily close by contraction. To study wound closure by granulation and re-epithelialization, as is relevant to humans, it is therefore required that cutaneous wounds be stented

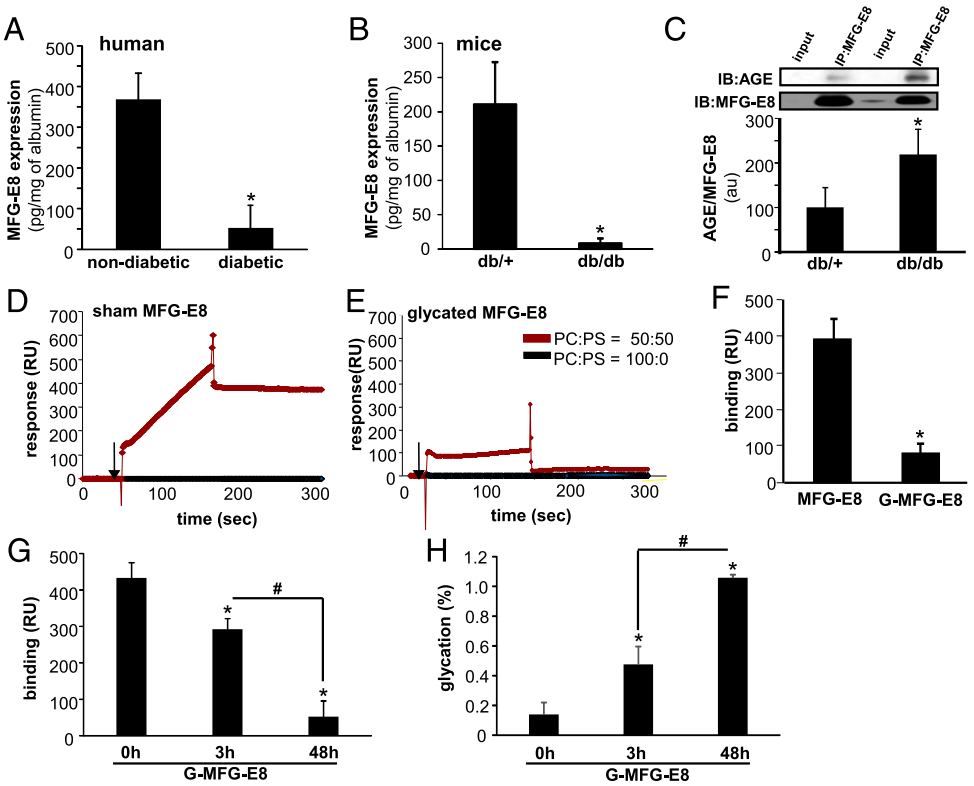

FIGURE 7. Lower MFG-E8 levels in the diabetic wound environment. (**A**) MFG-E8 protein levels in the wound fluids obtained from diabetic and nondiabetic chronic wounds (see Table I for subject demographics). MFG-E8 levels were determined using ELISA. Results are mean ± SD ($n = 5$). *$p <$ 0.05 compared with nondiabetic wound fluids. (**B**) Hunt–Schilling wire mesh cylinders were implanted s.c. in the back of diabetic ($Lepr^{db}$, db/db) or corresponding nondiabetic control (heterozygous, $Lepr^{db/+,}$ db/+) mice. Wound fluids were harvested day 3 postimplantation, and MFG-E8 level in wound fluids was determined using ELISA. Results are mean ± SD ($n = 4$). *$p < 0.05$ compared with db/+ wound fluids. (**C**) IP of MFG-E8 from day 3 wound-edge tissue lysates of diabetic (db/db) or corresponding nondiabetic control (db/+) mice. The IP was subjected to SDS-PAGE, followed by immunoblotting (IB) with anti-AGE Ab. Input represents cell lysates after IP reaction. Results are mean ± SD ($n = 4$). *$p < 0.05$ compared with db/+. (**D**–**F**) Surface plasmon resonance (SPR; Biacore) assay. Binding affinity was tested using SPR with PS or PC (control) liposomes immobilized on the sensor L1 chip and glycated MFG-E8 or sham MFG-E8 as soluble analytes. Glycation of MFG-E8 (G-MFG-E8) was achieved by incubating mouse rMFG-E8 (10 μg) with 10 mM MGO at 37˚C for 48 h, whereas sham MFG-E8 involved incubation with buffer at 37˚C for 48 h. The response curve of (D) sham MFG-E8 or (E) G-MFG-E8 binding with PS:PC (50:50) or PS:PC (0:100) liposomes has been presented. (F) The quantification of the binding has been presented as bar graph. Results are mean ± SD ($n = 3$). *$p < 0.05$ compared with sham MFG-E8. (**G**) Dose-dependent inhibition in binding affinity of G-MFG-E8 to PS as detected by Biacore SPR. The dose-dependent glycation of MFG-E8 was achieved by incubating MFG-E8 at 37˚C for 0, 3, and 48 h. Results are mean ± SD ($n = 3$). *$p < 0.05$ compared with 0 h, $^{\#}p < 0.05$ compared with 3 h. (**H**) Quantification of the level of glycation of MFG-E8 following 0, 3, or 48 h of exposure to MGO. The glycation of MFG-E8 was measured using glycoprotein carbohydrate estimation kit. Results are mean ± SD ($n = 4$). *$p < 0.05$ compared with 0 h, $^{\#}p < 0.05$ compared with 3 h.

(61). Marginal compromise in wound closure as reported in non-stented MFG-$E8^{-/-}$ mice may be attributed to the heavy influence of wound contraction, as opposed to healing, under such experimental conditions (17). Results reported from stented wounds in MFG-$E8^{-/-}$ mice in the current study demonstrate remarkable impairment in wound closure, recognizing MFG-E8 as a significant player in the overall healing process. Significance of such observation was further heightened by rescue experiments involving MFG-$E8^{-/-}$ mice that were subjected to wild-type BM transplantation. Also, transplantation of MFG-$E8^{-/-}$ BM to MFG-$E8^{+/+}$ mice compromised wound healing. Thus, this work provides definitive evidence establishing MFG-E8 as a critical contributor to the wound-healing process.

Mϕ are highly plastic and respond to environmental cues by adapting to classically activated (M1) proinflammatory or alternatively activated (M2) anti-inflammatory, proangiogenic phenotype (62, 63). Efferocytosis serves as a cue for mϕ switching to an anti-inflammatory and proangiogenic (M2) phenotype (7, 10, 11, 31, 64, 65). MFG-E8 has profound influence in promoting VEGF-induced angiogenesis (16, 17). Given that tissue mϕ have been directly implicated in angiogenesis (66, 67), the question as to whether mϕ-dependent mechanisms are involved in executing the angiogenic functions of MFG-E8 remains open. The current work demonstrates that, in cutaneous wounds of MFG-$E8^{-/-}$ mice, featuring persistent inflammation, wound angiogenesis is markedly compromised. Rescue experiments involving BM transplantation add clarity to this important observation. In light of a central role of MFG-E8 in driving efferocytosis and thereby switching wound-site mϕ toward an anti-inflammatory and proangiogenic form (M2), it is conceivable that the provascularization effects of MFG-E8 in the wound milieu may be dependent on its effects, supporting efferocytosis and downstream mϕ polarization. This contention was further substantiated by the observation that CM from wound mϕ from MFG-$E8^{+/+}$ mice displayed significantly improved angiogenic properties. Limited wound perfusion in a setting of persistent inflammation is commonly noted in diabetic ulcers. Whether limited MFG-E8 function is a causative factor complicating diabetic wound healing is therefore a reasonable question.

Previous work by our laboratory has recognized that an elevated apoptotic cell burden at wound site exaggerates sustained inflammation at the wound site (7). Furthermore, impaired efferocytosis by wound mϕ, increased apoptotic cell burden, and persistent inflammatory response is a hallmark of diabetic wounds

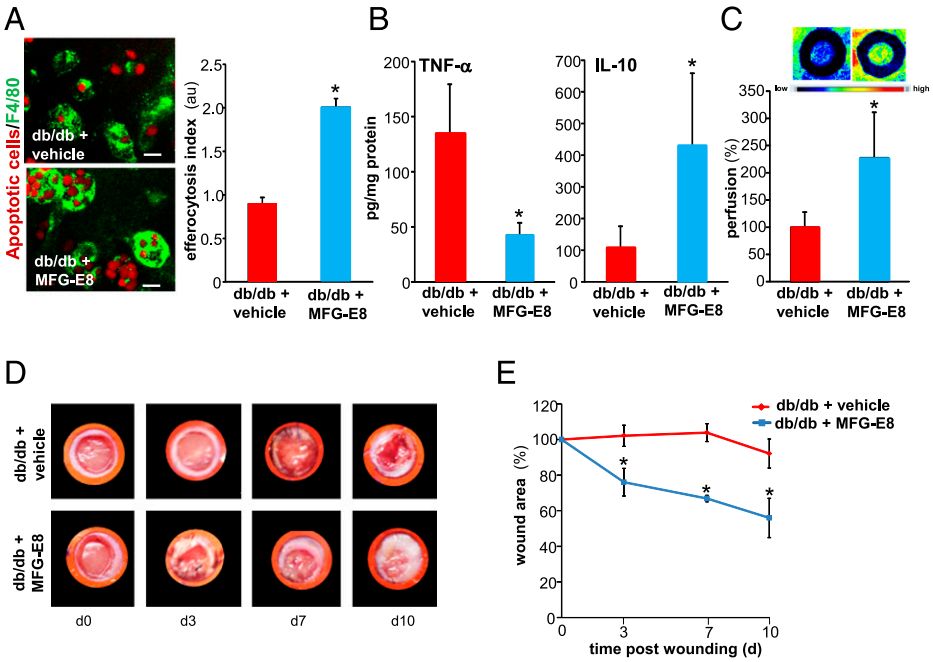

FIGURE 8. MFG-E8 treatment improves efferocytosis, angiogenesis, and healing in diabetic wounds. (**A**) Efferocytosis activity in day 3 wound mϕ harvested from db/db animals. Freshly isolated wound mϕ were incubated with rMFG-E8 (1 μg/ml) 2 h prior to subjecting them to efferocytosis in the presence of rMFG-E8 (1 μg/ml) or vehicle. Representative images of mϕ (F4/80, green) cocultured with apoptotic cells (pHrodo, red). Scale bar, 10 μm. Efferocytosis index was calculated, and data were presented as mean ± SD ($n = 4$). *$p < 0.05$ compared with vehicle-treated group. (**B**–**E**) Full-thickness dorsal wounds were created using a 6-mm biopsy punch on dorsal side of diabetic ($Lepr^{db}$, db/db) or corresponding nondiabetic control (heterozygous, $Lepr^{db/+,}$ db/+) mice. The wounds were stented and left to heal by secondary intention. Each wound was treated with either mouse rMFG-E8 (1 μg per wound in 50% glycerol/saline once daily) or equivalent amount of vehicle (mouse serum in 50% glycerine/saline once daily) for 10 d. (B) Quantification of TNF-α and IL-10 measured by ELISA in the day 10 wound-edge tissues. Data are expressed as mean ± SD ($n = 3$). *$p < 0.05$ compared with vehicle-treated wounds. (C) Laser speckle images from day 5 wounds. Bar graph presents quantification of the laser speckle analysis. Data presented as mean ± SD ($n = 4$). *$p < 0.05$ compared with control mice. (D) Representative wound images on day 0–10 postwounding; (E) wound area measurements were done using digital planimetry. Data are expressed as mean ± SD ($n = 3$). *$p < 0.05$ as compared with vehicle-treated db/db mice.

(7, 10, 11). Results of the present work uphold deficiencies in MFG-E8 functioning as a key factor explaining impaired efferocytosis and resulting in persistent inflammation in diabetic wounds. In diabetes, hyperglycemia is known to cause nonenzymatic glycation of free amino groups of proteins, which then leads to the structural and functional changes in these proteins, resulting in changes in functionality (68). The irreversible formation of advanced glycation end products (AGEs) is one example that is known to drive numerous pathophysiological mechanisms relevant to diabetic complications (69). In MFG-E8, unique structural characteristics such as the presence of RGD and proline/threonine-rich domains make it susceptible to glycation. Indeed, MGO, a precursor molecule for AGE, is present at high levels in diabetic plasma (70). MGO is a potent arginine-directed glycating agent that forms hydroimidazolone derivative Nδ-(5-hydro-5-methyl-4-imidazolon-2-yl)-ornithine residue with arginine (71). Nδ-(5-hydro-5-methyl-4-imidazolon-2-yl)-ornithine, an AGE, is a product of glycation abundant in diabetes (71). This work study provides maiden evidence demonstrating that MFG-E8 is not only sensitive to glycation in diabetic wounds also as predicted by its structure, but that glycation has a major impact on MFG-E8 function. That glycated MFG-E8 suffers from loss of binding activity toward PS, resulting in impaired efferocytosis by diabetic wound mϕ, is of substantial significance addressing chronic inflammation and poor perfusion commonly noted in diabetic ulcers. From a therapeutic standpoint, this work presents topical application of rMFG-E8 as a productive approach to circumvent blockade in the functioning of glycated endogenous MFG-E8. From a mechanistic standpoint, this finding highlights the importance of rescuing efferocytosis in diabetic wounds.

Wound-healing biology has always been viewed as a continuum of multiple processes that act in a synergistic and coordinated manner to achieve closure of the defect. Although processes such as inflammation, angiogenesis, and re-epithelialization are often studied as separated pieces for the sake of gaining traction in a somewhat simplified scenario, there is little doubt that these processes engage in sophisticated cross-talk and that such interplay is critical to achieving successful healing. This work recognizes mϕ-derived MFG-E8 as an influential commander of such cross-talk positioned at the seams of inflammation, angiogenesis, and re-epithelialization. Effective dead cell clearance at the wound site, enabled by MFG-E8, advances mϕ toward resolution of inflammation. Such resolution of inflammation in turn advances wound angiogenesis. As it relates to angiogenesis, MFG-E8 is capable of bolstering signaling of VEGF, helping perfuse the wound tissue. Resolution of inflammation together with effective wound vascularization supports re-epithelialization and wound closure. Above and beyond positioning MFG-E8 as master of a key hub in wound healing, this work recognizes that MFG-E8 may become defunct under conditions of hyperglycemia and exposure to AGE. Indeed, loss of MFG-E8 function impairs diabetic wound healing. From a therapeutic standpoint, it is of extraordinary interest that topical application of rMFG-E8 is effective in restoring MFG-E8 function in diabetic wounds. Topical rMFG-E8 induced resolution of wound inflammation, improvements in angiogenesis, and acceleration of closure, upholding the potential of MFG-E8–directed therapeutics in diabetic wound care.

Disclosures

The authors have no financial conflicts of interest.

References

1. Sen, C. K., G. M. Gordillo, S. Roy, R. Kirsner, L. Lambert, T. K. Hunt, F. Gottrup, G. C. Gurtner, and M. T. Longaker. 2009. Human skin wounds: a major and snowballing threat to public health and the economy. *Wound Repair Regen.* 17: 763–771.
2. Falanga, V. 2005. Wound healing and its impairment in the diabetic foot. *Lancet* 366: 1736–1743.
3. Pierce, G. F. 2001. Inflammation in nonhealing diabetic wounds: the space-time continuum does matter. *Am. J. Pathol.* 159: 399–403.
4. Brem, H., and M. Tomic-Canic. 2007. Cellular and molecular basis of wound healing in diabetes. [comment] *J. Clin. Invest.* 117: 1219–1222.
5. Eming, S. A., T. Krieg, and J. M. Davidson. 2007. Inflammation in wound repair: molecular and cellular mechanisms. *J. Invest. Dermatol.* 127: 514–525.
6. Serhan, C. N. 2009. Systems approach to inflammation resolution: identification of novel anti-inflammatory and pro-resolving mediators. *J. Thromb. Haemost.* 7 (Suppl. 1): 44–48.
7. Khanna, S., S. Biswas, Y. Shang, E. Collard, A. Azad, C. Kauh, V. Bhasker, G. M. Gordillo, C. K. Sen, and S. Roy. 2010. Macrophage dysfunction impairs resolution of inflammation in the wounds of diabetic mice. *PLoS One* 5: e9539.
8. Goren, I., N. Allmann, N. Yogev, C. Schürmann, A. Linke, M. Holdener, A. Waisman, J. Pfeilschifter, and S. Frank. 2009. A transgenic mouse model of inducible macrophage depletion: effects of diphtheria toxin-driven lysozyme M-specific cell lineage ablation on wound inflammatory, angiogenic, and contractive processes. *Am. J. Pathol.* 175: 132–147.
9. Mirza, R., L. A. DiPietro, and T. J. Koh. 2009. Selective and specific macrophage ablation is detrimental to wound healing in mice. *Am. J. Pathol.* 175: 2454–2462.
10. Roy, S., ed. 2010. *Resolution of Inflammation in Wound Healing: Significance of Dead Cell Clearance.* Mary Ann Liebert, New York.
11. Das, A., and S. Roy. 2013. Resolution of inflammation. In *Chronic Inflammation: Molecular Pathophysiology, Nutritional and Therapeutic Interventions.* D. B. S. Roy, and S. P. Raychaudhuri, eds. CRC Press, Boca Raton, FL, p. 119–128.
12. Serhan, C. N., S. D. Brain, C. D. Buckley, D. W. Gilroy, C. Haslett, L. A. O'Neill, M. Perretti, A. G. Rossi, and J. L. Wallace. 2007. Resolution of inflammation: state of the art, definitions and terms. *FASEB J.* 21: 325–332.
13. Maskrey, B. H., I. L. Megson, P. D. Whitfield, and A. G. Rossi. 2011. Mechanisms of resolution of inflammation: a focus on cardiovascular disease. *Arterioscler. Thromb. Vasc. Biol.* 31: 1001–1006.
14. Yamazaki, M., S. Maruyama, T. Abé, A. Essa, H. Babkair, J. Cheng, and T. Saku. 2014. MFG-E8 expression for progression of oral squamous cell carcinoma and for self-clearance of apoptotic cells. *Lab. Invest.* 94: 1260–1272.
15. Hanayama, R., M. Tanaka, K. Miwa, A. Shinohara, A. Iwamatsu, and S. Nagata. 2002. Identification of a factor that links apoptotic cells to phagocytes. *Nature* 417: 182–187.
16. Silvestre, J. S., C. Théry, G. Hamard, J. Boddaert, B. Aguilar, A. Delcayre, C. Houbron, R. Tamarat, O. Blanc-Brude, S. Heeneman, et al. 2005. Lactadherin promotes VEGF-dependent neovascularization. *Nat. Med.* 11: 499–506.
17. Uchiyama, A., K. Yamada, S. Ogino, Y. Yokoyama, Y. Takeuchi, M. C. Udey, O. Ishikawa, and S. Motegi. 2014. MFG-E8 regulates angiogenesis in cutaneous wound healing. *Am. J. Pathol.* 184: 1981–1990.
18. Roy, S., R. Dickerson, S. Khanna, E. Collard, U. Gnyawali, G. M. Gordillo, and C. K. Sen. 2011. Particulate β-glucan induces TNF-α production in wound macrophages via a redox-sensitive NF-κβ-dependent pathway. *Wound Repair Regen.* 19: 411–419.
19. Hanayama, R., M. Tanaka, K. Miyasaka, K. Aozasa, M. Koike, Y. Uchiyama, and S. Nagata. 2004. Autoimmune disease and impaired uptake of apoptotic cells in MFG-E8-deficient mice. *Science* 304: 1147–1150.
20. Chan, Y. C., S. Roy, Y. Huang, S. Khanna, and C. K. Sen. 2012. The microRNA miR-199a-5p down-regulation switches on wound angiogenesis by derepressing the v-ets erythroblastosis virus E26 oncogene homolog 1-matrix metalloproteinase-1 pathway. *J. Biol. Chem.* 287: 41032–41043.
21. Roy, S., S. Khanna, C. Rink, S. Biswas, and C. K. Sen. 2008. Characterization of the acute temporal changes in excisional murine cutaneous wound inflammation by screening of the wound-edge transcriptome. *Physiol. Genomics* 34: 162–184.
22. Chan, Y. C., S. Roy, S. Khanna, and C. K. Sen. 2012. Downregulation of endothelial microRNA-200b supports cutaneous wound angiogenesis by desilencing GATA binding protein 2 and vascular endothelial growth factor receptor 2. *Arterioscler. Thromb. Vasc. Biol.* 32: 1372–1382.
23. Ganesh, K., A. Das, R. Dickerson, S. Khanna, N. L. Parinandi, G. M. Gordillo, C. K. Sen, and S. Roy. 2012. Prostaglandin E_2 induces oncostatin M expression in human chronic wound macrophages through Axl receptor tyrosine kinase pathway. *J. Immunol.* 189: 2563–2573.
24. Roy, S., S. Khanna, K. Nallu, T. K. Hunt, and C. K. Sen. 2006. Dermal wound healing is subject to redox control. *Mol. Ther.* 13: 211–220.
25. Wohleb, E. S., N. D. Powell, J. P. Godbout, and J. F. Sheridan. 2013. Stress-induced recruitment of bone marrow-derived monocytes to the brain promotes anxiety-like behavior. *J. Neurosci.* 33: 13820–13833.
26. Peake, K., J. Manning, C. A. Lewis, C. Barr, F. Rossi, and C. Krieger. 2015. Busulfan as a myelosuppressive agent for generating stable high-level bone marrow chimerism in mice. *J. Vis. Exp.* Available at: http://www.jove.com/archive/98/april-2015.
27. Goertz, O., C. Poettgen, A. Akbari, J. Kolbenschlag, S. Langer, M. Lehnhardt, M. Stuschke, and L. von der Lohe. 2015. New model for long-term investigations of cutaneous microcirculatory and inflammatory changes following irradiation. *J. Radiat. Res.* 56: 456–461.
28. Wohleb, E. S., D. B. McKim, D. T. Shea, N. D. Powell, A. J. Tarr, J. F. Sheridan, and J. P. Godbout. 2014. Re-establishment of anxiety in stress-sensitized mice is caused by monocyte trafficking from the spleen to the brain. *Biol. Psychiatry* 75: 970–981.
29. Lewis, C. A., J. Manning, C. Barr, K. Peake, R. K. Humphries, F. Rossi, and C. Krieger. 2013. Myelosuppressive conditioning using busulfan enables bone marrow cell accumulation in the spinal cord of a mouse model of amyotrophic lateral sclerosis. *PLoS One* 8: e60661.
30. Huynh, M. L., V. A. Fadok, and P. M. Henson. 2002. Phosphatidylserine-dependent ingestion of apoptotic cells promotes TGF-beta1 secretion and the resolution of inflammation. *J. Clin. Invest.* 109: 41–50.
31. Das, A., K. Ganesh, S. Khanna, C. K. Sen, and S. Roy. 2014. Engulfment of apoptotic cells by macrophages: a role of microRNA-21 in the resolution of wound inflammation. *J. Immunol.* 192: 1120–1129.
32. Roy, S., D. Patel, S. Khanna, G. M. Gordillo, S. Biswas, A. Friedman, and C. K. Sen. 2007. Transcriptome-wide analysis of blood vessels laser captured from human skin and chronic wound-edge tissue. *Proc. Natl. Acad. Sci. USA* 104: 14472–14477.
33. Shilo, S., S. Roy, S. Khanna, and C. K. Sen. 2008. Evidence for the involvement of miRNA in redox regulated angiogenic response of human microvascular endothelial cells. *Arterioscler. Thromb. Vasc. Biol.* 28: 471–477.
34. Yamaguchi, H., J. Takagi, T. Miyamae, S. Yokota, T. Fujimoto, S. Nakamura, S. Ohshima, T. Naka, and S. Nagata. 2008. Milk fat globule EGF factor 8 in the serum of human patients of systemic lupus erythematosus. *J. Leukoc. Biol.* 83: 1300–1307.
35. Roy, S., J. Driggs, H. Elgharably, S. Biswas, M. Findley, S. Khanna, U. Gnyawali, V. K. Bergdall, and C. K. Sen. 2011. Platelet-rich fibrin matrix improves wound angiogenesis via inducing endothelial cell proliferation. *Wound Repair Regen.* 19: 753–766.
36. Chan, Y. C., S. Khanna, S. Roy, and C. K. Sen. 2011. miR-200b targets Ets-1 and is down-regulated by hypoxia to induce angiogenic response of endothelial cells. *J. Biol. Chem.* 286: 2047–2056.
37. Gordillo, G. M., A. Biswas, S. Khanna, X. Pan, M. Sinha, S. Roy, and C. K. Sen. 2014. Dicer knockdown inhibits endothelial cell tumor growth via microRNA 21a-3p targeting of Nox-4. *J. Biol. Chem.* 289: 9027–9038.
38. Roy, S., S. Khanna, T. Rink, J. Radtke, W. T. Williams, S. Biswas, R. Schnitt, A. R. Strauch, and C. K. Sen. 2007. P21waf1/cip1/sdi1 as a central regulator of inducible smooth muscle actin expression and differentiation of cardiac fibroblasts to myofibroblasts. *Mol. Biol. Cell* 18: 4837–4846.
39. Jacobi, J., J. J. Jang, U. Sundram, H. Dayoub, L. F. Fajardo, and J. P. Cooke. 2002. Nicotine accelerates angiogenesis and wound healing in genetically diabetic mice. *Am. J. Pathol.* 161: 97–104.
40. Elgharably, H., S. Roy, S. Khanna, M. Abas, P. Dasghatak, A. Das, K. Mohammed, and C. K. Sen. 2013. A modified collagen gel enhances healing outcome in a preclinical swine model of excisional wounds. *Wound Repair Regen.* 21: 473–481.
41. Roy, S., S. Khanna, A. Azad, R. Schnitt, G. He, C. Weigert, H. Ichijo, and C. K. Sen. 2010. Fra-2 mediates oxygen-sensitive induction of transforming growth factor beta in cardiac fibroblasts. *Cardiovasc. Res.* 87: 647–655.
42. Park, H. A., S. Khanna, C. Rink, S. Gnyawali, S. Roy, and C. K. Sen. 2009. Glutathione disulfide induces neural cell death via a 12-lipoxygenase pathway. *Cell Death Differ.* 16: 1167–1179.
43. He, M., H. Kubo, K. Morimoto, N. Fujino, T. Suzuki, T. Takahasi, M. Yamada, M. Yamaya, T. Maekawa, Y. Yamamoto, and H. Yamamoto. 2011. Receptor for advanced glycation end products binds to phosphatidylserine and assists in the clearance of apoptotic cells. *EMBO Rep.* 12: 358–364.
44. Small, H., I. Gardner, H. M. Jones, J. Davis, and M. Rowland. 2011. Measurement of binding of basic drugs to acidic phospholipids using surface plasmon resonance and incorporation of the data into mechanistic tissue composition equations to predict steady-state volume of distribution. *Drug Metab. Dispos.* 39: 1789–1793.
45. Fadok, V. A., D. L. Bratton, A. Konowal, P. W. Freed, J. Y. Westcott, and P. M. Henson. 1998. Macrophages that have ingested apoptotic cells in vitro inhibit proinflammatory cytokine production through autocrine/paracrine mechanisms involving TGF-beta, PGE2, and PAF. *J. Clin. Invest.* 101: 890–898.
46. Rath, M., I. Müller, P. Kropf, E. I. Closs, and M. Munder. 2014. Metabolism via arginase or nitric oxide synthase: two competing arginine pathways in macrophages. *Front. Immunol.* 5: 532.
47. Cohen, P. L., R. Caricchio, V. Abraham, T. D. Camenisch, J. C. Jennette, R. A. Roubey, H. S. Earp, G. Matsushima, and E. A. Reap. 2002. Delayed apoptotic cell clearance and lupus-like autoimmunity in mice lacking the c-mer membrane tyrosine kinase. *J. Exp. Med.* 196: 135–140.
48. Seitz, H. M., T. D. Camenisch, G. Lemke, H. S. Earp, and G. K. Matsushima. 2007. Macrophages and dendritic cells use different Axl/Mertk/Tyro3 receptors in clearance of apoptotic cells. *J. Immunol.* 178: 5635–5642.
49. Nishi, C., S. Toda, K. Segawa, and S. Nagata. 2014. Tim4- and MerTK-mediated engulfment of apoptotic cells by mouse resident peritoneal macrophages. *Mol. Cell. Biol.* 34: 1512–1520.
50. Todt, J. C., B. Hu, and J. L. Curtis. 2004. The receptor tyrosine kinase MerTK activates phospholipase C gamma2 during recognition of apoptotic thymocytes by murine macrophages. *J. Leukoc. Biol.* 75: 705–713.
51. Elgharably, H., K. Ganesh, J. Dickerson, S. Khanna, M. Abas, P. D. Ghatak, S. Dixit, V. Bergdall, S. Roy, and C. K. Sen. 2014. A modified collagen gel dressing promotes angiogenesis in a preclinical swine model of chronic ischemic wounds. *Wound Repair Regen.* 22: 720–729.

52. Weisser, S. B., K. W. McLarren, E. Kuroda, and L. M. Sly. 2013. Generation and characterization of murine alternatively activated macrophages. *Methods Mol. Biol.* 946: 225–239.
53. Springer, M. L., T. K. Ip, and H. M. Blau. 2000. Angiogenesis monitored by perfusion with a space-filling microbead suspension. *Mol. Ther.* 1: 82–87.
54. Li, B. Z., H. Y. Zhang, H. F. Pan, and D. Q. Ye. 2013. Identification of MFG-E8 as a novel therapeutic target for diseases. *Expert Opin. Ther. Targets* 17: 1275–1285.
55. Raymond, A., M. A. Ensslin, and B. D. Shur. 2009. SED1/MFG-E8: a bi-motif protein that orchestrates diverse cellular interactions. *J. Cell. Biochem.* 106: 957–966.
56. Otani, A., S. Ishihara, M. M. Aziz, N. Oshima, Y. Mishima, I. Moriyama, T. Yuki, Y. Amano, M. M. Ansary, and Y. Kinoshita. 2012. Intrarectal administration of milk fat globule epidermal growth factor-8 protein ameliorates murine experimental colitis. *Int. J. Mol. Med.* 29: 349–356.
57. Aziz, M., A. Jacob, A. Matsuda, R. Wu, M. Zhou, W. Dong, W. L. Yang, and P. Wang. 2011. Pre-treatment of recombinant mouse MFG-E8 downregulates LPS-induced TNF-α production in macrophages via STAT3-mediated SOCS3 activation. *PLoS One* 6: e27685.
58. Miksa, M., R. Wu, W. Dong, P. Das, D. Yang, and P. Wang. 2006. Dendritic cell-derived exosomes containing milk fat globule epidermal growth factor-factor VIII attenuate proinflammatory responses in sepsis. *Shock* 25: 586–593.
59. Leibovich, S. J., and R. Ross. 1975. The role of the macrophage in wound repair: a study with hydrocortisone and antimacrophage serum. *Am. J. Pathol.* 78: 71–100.
60. Motegi, S., W. W. Leitner, M. Lu, Y. Tada, M. Sárdy, C. Wu, T. Chavakis, and M. C. Udey. 2011. Pericyte-derived MFG-E8 regulates pathologic angiogenesis. *Arterioscler. Thromb. Vasc. Biol.* 31: 2024–2034.
61. Galiano, R. D., J. Michaels, V, M. Dobryansky, J. P. Levine, and G. C. Gurtner. 2004. Quantitative and reproducible murine model of excisional wound healing. *Wound Repair Regen.* 12: 485–492.
62. Das, A., M. Sinha, S. Datta, M. Abas, S. Chaffee, C. K. Sen, and S. Roy. 2015. Monocyte and macrophage plasticity in tissue repair and regeneration. *Am. J. Pathol.* 185: 2596–2606.
63. Sen, C. K. 2015. Expanding horizons of cellular plasticity in regenerative medicine. *Am. J. Pathol.* 185: 2592–2595.
64. Korns, D., S. C. Frasch, R. Fernandez-Boyanapalli, P. M. Henson, and D. L. Bratton. 2011. Modulation of macrophage efferocytosis in inflammation. *Front. Immunol.* 2: 57.
65. Filardy, A. A., D. R. Pires, M. P. Nunes, C. M. Takiya, C. G. Freire-de-Lima, F. L. Ribeiro-Gomes, and G. A. DosReis. 2010. Proinflammatory clearance of apoptotic neutrophils induces an IL-12(low)IL-10(high) regulatory phenotype in macrophages. *J. Immunol.* 185: 2044–2050.
66. Nucera, S., D. Biziato, and M. De Palma. 2011. The interplay between macrophages and angiogenesis in development, tissue injury and regeneration. *Int. J. Dev. Biol.* 55: 495–503.
67. Rahat, M. A., B. Hemmerlein, and V. Iragavarapu-Charyulu. 2014. The regulation of angiogenesis by tissue cell-macrophage interactions. *Front. Physiol.* 5: 262.
68. Friedman, E. A. 1999. Advanced glycosylated end products and hyperglycemia in the pathogenesis of diabetic complications. *Diabetes Care* 22(Suppl. 2): B65–B71.
69. Huijberts, M. S., N. C. Schaper, and C. G. Schalkwijk. 2008. Advanced glycation end products and diabetic foot disease. *Diabetes Metab. Res. Rev.* 24(Suppl. 1): S19–S24.
70. McLellan, A. C., P. J. Thornalley, J. Benn, and P. H. Sonksen. 1993. Modification of the glyoxalase system in clinical diabetes mellitus. *Biochem. Soc. Trans.* 21: 158S.
71. Dobler, D., N. Ahmed, L. Song, K. E. Eboigbodin, and P. J. Thornalley. 2006. Increased dicarbonyl metabolism in endothelial cells in hyperglycemia induces anoikis and impairs angiogenesis by RGD and GFOGER motif modification. *Diabetes* 55: 1961–1969.